

# RF field amplitudes in the SOL and far-field RF sheaths: a proposed mechanism for the anomalous loss of RF power to the SOL of NSTX

R. J. Perkins<sup>1</sup>, J. C. Hosea<sup>1</sup>, N. Bertelli<sup>1</sup>, J.-W. Ahn<sup>2</sup>, R. E. Bell<sup>1</sup>, A. Diallo<sup>1</sup>, S. Gerhardt<sup>1</sup>, T. K. Gray<sup>2</sup>, J. C. Hosea<sup>1</sup>, M. A. Jaworski<sup>1</sup>, B. P. LeBlanc<sup>1</sup>, G. J. Kramer<sup>1</sup>, A. McLean<sup>3</sup>, R. Maingi<sup>1</sup>, L. Roquemore<sup>1</sup>, S. Sabbagh<sup>4</sup>, G. Taylor<sup>1</sup> and J. R. Wilson<sup>1</sup>

<sup>1</sup>Princeton Plasma Physics Laboratory, Princeton, USA

<sup>2</sup>Oak Ridge National Laboratory, Oak Ridge, USA

<sup>3</sup>Lawrence Livermore National Laboratory, Livermore, USA

<sup>4</sup>Columbia University, New York, USA

*Corresponding Author:* rperkins@pppl.gov

## Abstract:

We propose a new model for the anomalous loss of high-harmonic fast-wave (HHFW) heating power to the scrape-off layer (SOL) of the National Spherical Torus eXperiment (NSTX). A significant fraction, up to 60%, of the coupled HHFW power can be lost along scrape-off layer field lines, creating bright spirals of heat deposition on the upper and lower divertor regions. It is important to determine the underlying mechanism because, with 20 MW of ICRF power planned for ITER, a similar loss of ICRF power may erode the divertor and produce unacceptable impurity levels. We hypothesize that the SOL losses are caused by a two-step process. First, the radiofrequency (RF) field amplitude becomes quite high in the SOL when the right-hand fast-wave cutoff layer is positioned too close to the HHFW antenna. Second, these RF fields setup far-field RF sheaths on the divertor tiles and drive an enhanced heat flux into the divertor. We present results from a cylindrical cold-plasma model that demonstrate a class of modes that conduct a significant fraction of their wave power in the peripheral plasma; these modes appear when a half radial wavelength fits into the SOL. Experimental evidence for RF rectified voltages and currents is presented, and our analysis suggests that they could produce additional heat fluxes consistent with infrared camera measurements of the HHFW heat flux within the spirals. This suggests that the SOL losses can be minimized, and heating efficiency maximized, through tailoring of SOL density and antenna phasing, which will be an important consideration for high-power long-pulse ICRF heating on fusion devices, such as ITER.

## 1 Introduction

Losses of high-harmonic fast-wave (HHFW) power to the scrape-off layer (SOL) of the National Spherical Torus Experiment (NSTX) is a significant operational issue [1]. Multi-

megawatt electron heating via HHFW provides an alternate heating scheme to neutral-beam injection without particle or momentum input and has previously been exploited for transport studies [2], formation of electron internal transport barriers [3], and influencing Alfvénic eigenmode activity [4]. SOL losses of lower hybrid power have also been observed on Alcator C-Mod [5]. Finally, 20 MW of ion-cyclotron heating power is planned for ITER, so edge losses there could be an issue in terms of erosion or impurity production. In this paper, we propose that the SOL HHFW losses on NSTX are caused by a two-step process. First, the RF amplitude in the SOL is enhanced due to cavity-like modes that appear when the density in front of the antenna is large enough such that fast-waves propagate in that region out to the vicinity of the antenna. Here, this phenomenon is explored using a cylindrical cold-plasma model, which shows a class of modes with large HHFW amplitudes outside the core plasma. Second, these enhanced fields drive enhanced sheath losses via RF rectification. Calculations using probe data from the NSTX divertor indicate that such sheath losses can be substantial.

The HHFW regime may be susceptible to producing unusually large RF field amplitudes in the SOL. This was first proposed in observation of how the heating efficiency depended strongly on the toroidal wavenumber,  $k_\phi$ , edge density and magnetic field strength in a manner reminiscent of the cutoff density for fast-wave propagation [1]. Subsequent simulations using the full-wave code AORSA showed that, as the density in front of the antenna was raised above this cutoff value, there was an abrupt increase in RF field amplitude in the SOL [6, 7]. In order to address the fundamental physics behind this phenomena, we developed a cylindrical cold-plasma model, in which a special class of modes was found that exhibit an abnormal flux of wave power outside the core plasma [8]. The condition for such a mode to exist is that a half radial wavelength fits into the edge region. Present work is focused on the behavior of the annulus resonance on the azimuthal wavenumber and how these modes sum together to give the full three-dimensional reconstructed field pattern.

RF rectification is currently the leading candidate for explaining how the HHFW power flux is converted to a heat flux on the divertor. Signatures of rectified electron currents have been observed on divertor probes on NSTX only when the spiral lies over the probes [9], suggesting that substantial RF fields are propagating to this region. RF rectification is typically studied at the antenna itself in connection with impurity production, hot spot formation, or SOL modifications, and it is typically assumed that the plasma potential rises to neutralize any rectified electron current. Thus, the NSTX case offers a somewhat unconventional regime for RF rectification, although we note that rectified currents have long been observed [10]. First-principle calculations show that rectified current delivers a substantial heat flux to the surface, and that this is likely a conservative estimate.

## 2 Annulus Resonances in Cylindrical Plasmas

The high-harmonic fast-wave regime may produce abnormally large RF fields in the SOL. While the reason behind this is still not definitively determined, it has long been hypoth-

esized to onset when the plasma in front of the antenna supports fast-wave propagation (as opposed to the more typical scenario in ICRF operation where there is an evanescent region in front of the antenna). In the following section, we present results from a cylindrical cold-plasma model which shows a special class of modes, so called “annulus resonances,” which exhibit a large fraction of wave power propagating outside the core plasma. These modes are natural candidates to explain the losses on NSTX, and current work is focused on summing these modes over azimuthal wavenumber to produce the full three-dimensional fields.

The original cylindrical model is discussed in detail in Ref. [8]. It consists of three radial regions: a core plasma that extends to radius  $r_c$  with constant density  $n_c$ , a lower-density annulus that extends from  $r=r_c$  to  $r_a$  with constant density  $n_a$ , and an outer vacuum region which extends to a conducting wall of radius  $r_w$ . A uniform axial magnetic field is used throughout. The coarse step profile is partially justified in that NSTX H-mode discharges have a relatively short density length scale of 1-2 cm at the separatrix [11] whereas the perpendicular fast-wave wavelength in the SOL is typically larger, for instance, 26 cm for a nominal SOL density of  $2 \times 10^{18} \text{ m}^{-3}$  and 7.9 cm at a nominal separatrix density of  $10^{19} \text{ m}^{-3}$ , both at current-drive phasing. The antenna is modelled as current straps in the  $\theta$  direction at  $r = r_s$  with a Faraday screen at  $r = r_F$ . We chose NSTX-like parameters:  $n_c = 5 \times 10^{19} \text{ m}^{-3}$ ,  $f = 30 \text{ MHz}$ ,  $B = 0.32 \text{ T}$  (approximate field at the edge for a 0.55 T on-axis field),  $r_c = 0.515 \text{ m}$ ,  $r_a = 0.575 \text{ m}$ ,  $r_F = 0.600 \text{ m}$ ,  $r_s = 0.650 \text{ m}$ , and  $r_w = 0.700 \text{ m}$ . For a given azimuthal modenummer  $m$ , the model admits a finite number of modes: global solutions of the form  $\tilde{E}_z(r, m, k_{\parallel}) = \tilde{E}_z(r) \exp(im\theta + ik_{\parallel}z - i\omega t)$  that satisfy the wave equation in each region and are matched at interfaces. With  $k_{\parallel}$  specified,  $k_{\perp}$  is fixed in each region by the cold-plasma dispersion. The details of determining the  $k_{\parallel}$  of each mode is detailed in Ref. [8], but in general each mode fits an integral number of half-wavelengths in the radial region in  $E_{\theta}$ .

Annulus resonant modes have three main characteristics: (1) they fit half a radial wavelength structure into the combined annulus-vacuum region, (2) they have a relatively large loading resistance compared to other modes in the system, and (3) they propagate a significant fraction, sometimes over 50%, of the wave power outside the core plasma. When the loading resistance of all modes present in the system is plotted against the  $k_{\parallel}$  of the mode, the annulus resonance forms a peak in an otherwise smooth curve. This is shown for  $m = 2$  modes in Fig. 1a for several different values of annulus density. In this figure, the antenna current density is set to  $J = I_0\delta(z)$  so that all modes are weighted equally for ease of comparison. As the annulus density increases, the  $k_{\parallel}$  value of the annulus resonance increases to hold the phase difference across the annulus-vacuum region to  $\pi/2$ , as  $k_{\perp}$  in the annulus increases with  $n_a$  but decreases with  $k_{\parallel}$  for fast waves. At high enough density ( $n_a = 1 \times 10^{19} \text{ m}^{-3}$ ), an additional annulus resonance appears corresponding to three-halves of a wavelength fitting into the annulus-vacuum region. Figure 1b shows how the wave power is partitioned between the three cross-sections in the model for each mode of the  $n_a = 3 \times 10^{18} \text{ m}^{-3}$  case from Fig. 1a. Most modes conduct nearly all their wave power in the core region except for the annulus resonance, for which over half the power is conducted in the relatively small annulus region. The term “annulus resonance” is rationalized by the sharp change in radial distribution of Poynting flux shown in this

figure.

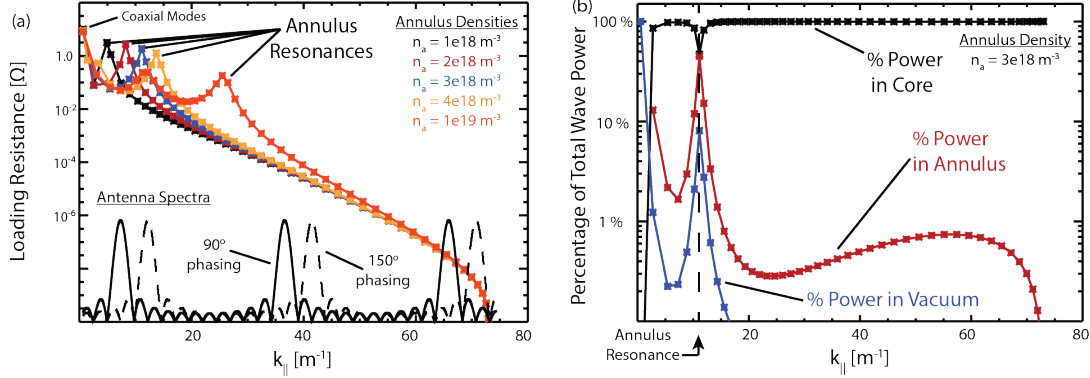


FIG. 1: (a) Loading resistance of  $m = 2$  modes for various annulus densities  $n_a$ . Antenna spectra for a model twelve-strap antenna with 21 cm inter-strap spacing and 90° and 150° phasing are plotted for reference. (b) Percentage of wave power conducted by each mode in the core (black), annulus (red), and vacuum (blue) regions for the case of  $n_a = 3 \times 10^{18} \text{ m}^{-3}$  case of (a). Figure 2 of Ref. [8].

### 3 RF Rectification in the Divertor of NSTX

RF rectification is the leading candidate for the mechanism converting HHFW power into a heat flux on the divertors. Present calculations suggest that, with the level of RF voltage estimated in the divertor, the heat flux to the divertor plates is substantially increased. This section reviews the experimental evidence for RF rectification and the calculations showing that the sheath dissipation is substantial.

#### 3.1 Evidence of RF Rectification

Early evidence for RF rectification was found in divertor Langmuir probes and Rogowski coils when these diagnostics lie underneath the spirals. The Langmuir probes showed a downward shift in floating potential, and the Rogowski coil showed an increase in collected electron current. A direct comparison is made in Fig. 2; Probe 1 is underneath the spiral and experiences the RF field there, whereas Probe 3 is not. The characteristic of Probe 1 appears shifted negative relative to Probe 3 with a minimal change in electron temperature. This is consistent with the theoretical prediction that an RF voltage  $V_{RF}$  would enhance the average electron current through the sheath.

$$I_{RF}^-(V) = I^{sat} I_0 \left( \frac{V_{RF}}{T_e} \right) \exp \left( \frac{V - V_{fl} - \Delta V_{pl}}{T_e} \right), \quad (1)$$

where  $V$  is the probe bias relative to vessel potential,  $I^{sat}$  is the ion saturation current, and  $\Delta V_{pl}$  is the change in plasma potential when the RF is applied (secondary electron emission

is suppressed here for simplicity). Setting  $\Delta V_{pl} = 0$  recovers the original formulation given in Ref. [12]. Studies of RF rectification, typically conducted in the vicinity of the antenna, often assume that  $\Delta V_{pl}$  rises enough to neutralize the increase in electron current, that is

$$V_{fl}^{RF} = T_e \ln I_0 \left( \frac{V_{RF}}{T_e} \right). \quad (2)$$

The NSTX divertor during HHFW heating demonstrates a regime in which the rectified currents are not fully neutralized. There are several possible explanations for this. First, at an antenna,  $V_{RF}$  may be one or two orders of magnitude larger than  $T_e$ , and one could not expect the exponential scaling of Eq. (1) to hold, but, in the divertor of NSTX,  $V_{RF}$  is only several times larger than  $T_e$ . Second, the flux tube linking a divertor probe has a long length over which cross-field diffusion can potentially alleviate electron depletion; this is not the case for certain antenna components, such as Faraday screen bars, which are connected over short lengths to other material surfaces [13].

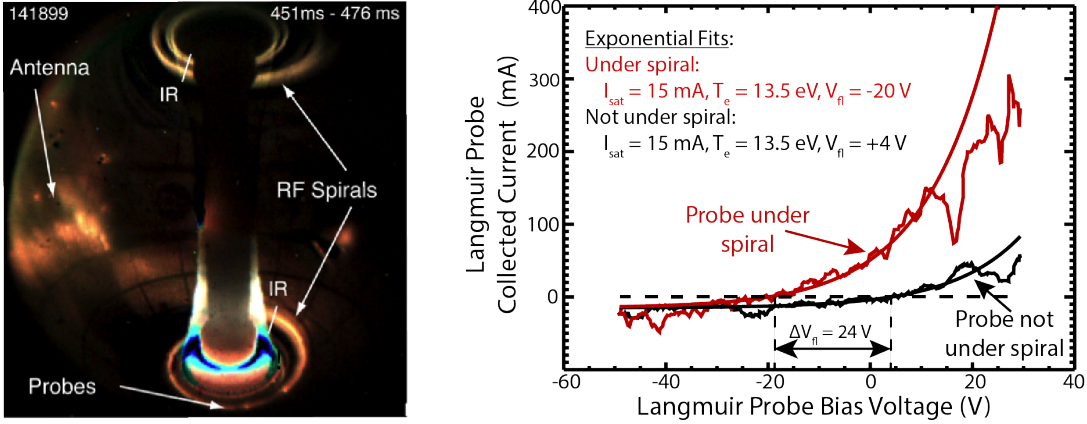


FIG. 2: (a) Divertor Langmuir probe floating potential and (b)  $T_e$  and  $I_{sat}$  as functions of applied HHFW during a power ramp.  $V_{fl}$  clearly changes initially but appears to clamp, whereas  $T_e$  and  $I_{sat}$  do not appear to change systematically.

It may be argued that an increase in SOL electron temperature would cause a similar downward shift in floating potential, which, in principle, is related to plasma potential via  $V_{fl} = V_{pl} - \alpha T_e$ , with  $\alpha$  of order unity. However, we have shown that, during an HHFW power ramp of duration 10 ms, the probe floating potential changes whereas the electron temperature and ion saturation current do not [14]. This is shown in Fig. 3

### 3.2 The Heat Flux Due to RF Rectification

Using first-principle calculations [15], one can derive the expected heat flux due to RF rectification [9]:

$$\Delta Q_{RF} = \Delta V_{pl} I^{sat} + 2 I^{sat} T_e e^{(V - V_{fl})/T_e} \left( I_0 \left( \frac{V_{RF}}{T_e} \right) e^{-\Delta V_{pl}/T_e} - 1 \right), \quad (3)$$

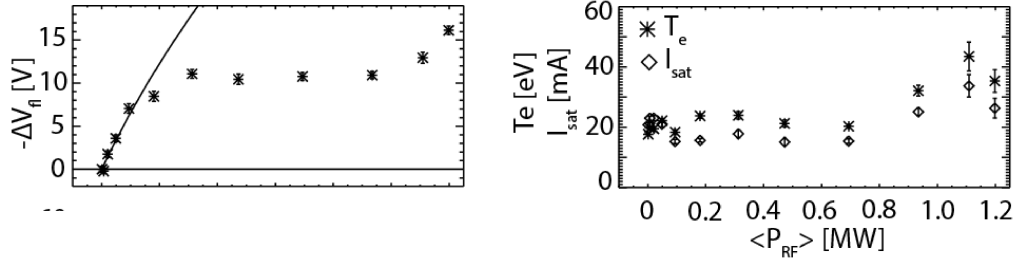


FIG. 3: (a) Divertor Langmuir probe floating potential and (b)  $T_e$  and  $I_{sat}$  as functions of applied HHFW during a power ramp.  $V_{fl}$  clearly changes initially but appears to clamp, whereas  $T_e$  and  $I_{sat}$  do not appear to change systematically.

where  $\Delta V_{pl}$  is the change in plasma potential.  $Q_{RF}$  consists of two components, ion bombardment due to ions increase of  $\Delta V_{pl}$  to the sheath potential drop, and an electron thermal component, which increases as in Eq. (1). The former is the term typically analyzed in ICRF studies to the exclusion of the latter, for reasons mentioned above. However, calculations taken from the NSTX divertor suggest that this term is extremely important in our application of HHFW losses in far-field sheaths.

If  $V_{RF}$  were given, we could analyze Eq. (3) in two extreme cases. In the first case, we could assume that there is no increase in plasma potential, giving

$$\Delta Q_{RF} = 2I^{sat}T_e e^{(V-V_{fl})/T_e} \left( I_0 \left( \frac{V_{RF}}{T_e} \right) - 1 \right), \quad (4)$$

In the second case, we could assume that the plasma potential,  $V_{pl}$  changes by an amount that exactly nullifies the rectified electron current, e.g. Eq. (2), and the heat flux is

$$\Delta Q_{RF} = \Delta V_{pl} J^{sat} = T_e J_{sat} \ln \left( I_0 \left( \frac{V_{RF}}{T_e} \right) \right). \quad (5)$$

In the limit  $V_{RF} \gg T_e$ , the latter gives a linear dependence of  $\Delta Q_{RF}$  on  $V_{RF}$ , while the former would give an exponentially growing dependence (which cannot be sustained for ever increasing  $V_{RF}$ , as discussed above).

The divertor Langmuir probes in NSTX need to be analyzed in a slightly different fashion, as the probes give the change in floating potential, but  $V_{RF}$  is not known a priori. As written, Eq. (3) depends on two variables,  $V_{RF}$  and  $\Delta V_{pl}$ , which act in opposite ways on the Langmuir probe characteristic:  $V_{RF}$  tending to shift the floating potential negative, and  $\Delta V_{pl}$  shifting the floating potential positive. The divertor Langmuir probes on NSTX measure the net change in floating potential but cannot resolve the individual contributions of  $V_{RF}$  and  $\Delta V_{pl}$ . The calculations performed in Ref. [9] assume that there is no change in plasma potential. This is actually the most conservative assumption for a given observed shift in floating potential [14]. Under this assumption, a substantial increase in sheath heat flux is predicted, as shown in Table I.

The obvious next step would be to measure the heat flux to the divertor and probes using infrared (IR) themography to provide an independent check of these measurements.

Shot	$P_{RF}$ [MW]	$T_e$ [eV]	$V_{fl}$ [V]	$V_{fl,RF}$ [V]	$\Delta\gamma_{RF}$	$\Delta\gamma_{RF,fl}$	$Q_{noRF}$ [MW/m <sup>2</sup> ]	$\Delta Q_{RF,rc}$ [MW/m <sup>2</sup> ]	$\Delta Q_{RF,rv}$ [MW/m <sup>2</sup> ]
141899	1.5	13.5	4	-20	7.3	1.8	0.1	0.21	0.13
141836	1.1	30	5	-23	2.5	0.92	0.35	0.49	0.5
141830	0.55	22.5	1	-10	2.8	0.49	0.37	0.44	0.38

TABLE I: PREDICTIONS BASED ON DIVERTOR LANGMUIR PROBE DATA. BOTH AS THE HEAT FLUX  $Q$  AND THE SHEATH HEAT TRANSMISSION COEFFICIENT  $\gamma = Q/J_{sat}T_e$ .

Unfortunately, in the NSTX data the viewing area of the IR cameras is toroidally separated from the probe array (Fig. 2a), and accurate comparisons cannot be made due to the strong variation of the spiral strength with toroidal angle. While rough estimates show that the probe predictions are comparable to extrapolations from the IR data [9], a definitive analysis will have to await data from NSTX-Upgrade. We also note that the NSTX divertor probe data is sampled from a weaker region of the spiral, so that the RF voltages and heat fluxes may be far greater when sampled at the most intense portion of the spiral.

## 4 Conclusion and directions for future work

To date the study of annulus resonances has been limited to individual modes of single azimuthal modenumbers, but the full field is a sum over all modes weighted by the antenna spectrum. Furthermore, while the annulus resonances do conduct significant power in the annulus, they also conduct significant power in the core and are thus susceptible to the strong core damping characteristic of high beta devices such as spherical tokamaks. We hypothesize that, when summing over modes, the highly oscillatory fields in the core will tend to cancel, but this remains to be seen. As it stands, though, the fact that modes with large field amplitudes in the edge appear in a cold-plasma model lends further evidence to the hypothesis that the SOL losses on NSTX are driven by a fast-wave propagation phenomenon.

RF rectification is the leading candidate for the mechanisms converting HHFW power into a heat flux on the surface. Further studies of RF rectification will likely require new experiments on NSTX-Upgrade with improved diagnostic coverage. This includes a new radial array of Langmuir probes with electronics to extract the 30 MHz signal. This array will be situated at the most intense portion of the spiral as well. A direct measurement of  $V_{RF}$  will alleviate many of the previously unresolvable ambiguities in analyzing RF rectification from NSTX data. Also, a wide-angle infrared camera will measure the heat flux at the probe location, providing an opportunity to validate the predicted dependence of this heat flux on  $V_{RF}$ . Future work may also include the installation of an emissive probe at the midplane to directly monitor changes in plasma potential during HHFW operation.

This work was supported by DOE Contract No. DE-AC02-09CH11466.

## References

- [1] Hosea, J., et al. “High harmonic fast wave heating efficiency enhancement and current drive at longer wavelength on the National Spherical Torus Experimental.” *Phys. Plasmas* 15 (2008) 056104.
- [2] Mazzucato, E., et al. “Short-scale turbulent fluctuations driven by the electron-temperature gradient in the National Spherical Torus Experiment.” *Phys. Rev. Lett.* 101 (2008) 075001.
- [3] Yuh, H. Y., et al. “Internal transport barriers in the National Spherical Torus Experiment.” *Physics of Plasmas* 16 (2009) 056120.
- [4] Fredrickson, E., et al. “Suppression of energetic particle driven instabilities with hhfw heating.” *Nuclear Fusion* 55 (2015) 013012.
- [5] Wallace, G. M., et al. these proceedings.
- [6] Green, D. L., et al. “Predicting high harmonic ion cyclotron heating efficiency in tokamak plasmas.” *Phys. Rev. Lett.* 107 (2011) 145001.
- [7] Bertelli, N., et al. “Full wave simulations of fast wave heating losses in the scrape-off layer of NSTX and NSTX-U.” *Nuclear Fusion* 54 (2014) 083004.
- [8] Perkins, R. J., et al. “Resonance in fast-wave amplitude in the periphery of cylindrical plasmas and application to edge losses of wave heating power in tokamaks.” *Physics of Plasmas* 23 (2016) 070702.
- [9] Perkins, R. J., et al. “The contribution of radio-frequency rectification to field-aligned losses of high-harmonic fast wave power to the divertor in the National Spherical Torus eXperiment.” *Phys. Plasmas* 22.
- [10] Nieuwenhove, R. V., Oost, G. V. “Experimental evidence for sheath effects at the ICRF antenna and ensuing changes in the plasma boundary during ICRF on TEXTOR.” *Journal of Nuclear Materials* 162 (1989) 288 .
- [11] Zweben, S. J., et al. “Blob structure and motion in the edge of NSTX.” *Plasma Phys. and Controlled Fusion* 58 (2016) 044007.
- [12] Boschi, A., Magistrelli, F. “Effect of a R.F. signal on the characteristic of a Langmuir probe.” *Il Nuovo Cimento* 29 (1963) 487.
- [13] Perkins, F. “Radiofrequency sheaths and impurity generation by ICRF antennas.” *Nuclear Fusion* 29 (1989) 583.
- [14] Perkins, R. J., et al. submitted to *Journal of Nuclear Materials and Energy*
- [15] Stangeby, P. C. *The Plasma Boundary of Magnetic Fusion Devices*, (Plasma Physics Series (Taylor and Francis Group)2000).